INTERNATIONAL ATOMIC ENERGY AGENCY
UNITED NATIONS EDUCATIONAL, SCIENTIFIC AND CULTURAL ORGANIZATION

INTERNATIONAL CENTRE FOR THEORETICAL PHYSICS
34100 TRIESTE (ITALY) - P.O.B. 586 - MIRAMARE - STRADA COSTIERA 11 - TELEPHONES: 224281/2/3/4/5/6
CABLE: CENTRATOM - TELEX 460392-1

SMR/115 - 47

WINTER COLLEGE ON LASERS, ATOMIC AND MOLECULAR PHYSICS

(21 January - 22 March 1985)

LASER SPECTROSCOPY & THEORY OF SPHERICAL TOP MOLECULES

J. BORDÉ
Département de Physique
Université de Paris-Nord
Villetaneuse
France

Ultra high resolution infrared spectra of small polyatomic molecules : the saturation spectroscopy of SF_6

Jacques Bordé.

Laboratoire de Physique des Lasers
Université Paris-Nord
93430 - VILLETANEUSE (FRANCE)

Introduction.

With the advent of lasers, a lot of new spectroscopic methods have been developped, taking advantage of the monochromaticity of the source, of its power and of the possibility of very short pulses. Among these techniques, the saturated absorption spectroscopy (SAS) has been improved for now 15 years and is now giving outstanding new information about molecules. Although the idea and the first demonstration of SAS took place around 1970, it took several years to build saturation spectrometers and to improve them by reducing all the factors still limiting the resolution ; during these years, the equations describing the interaction between light and matter during such a non-linear process were better understood and solved and the causes of line-broadening could be identified and better controlled in the experimental set-up. Because of SAS, the resolution has

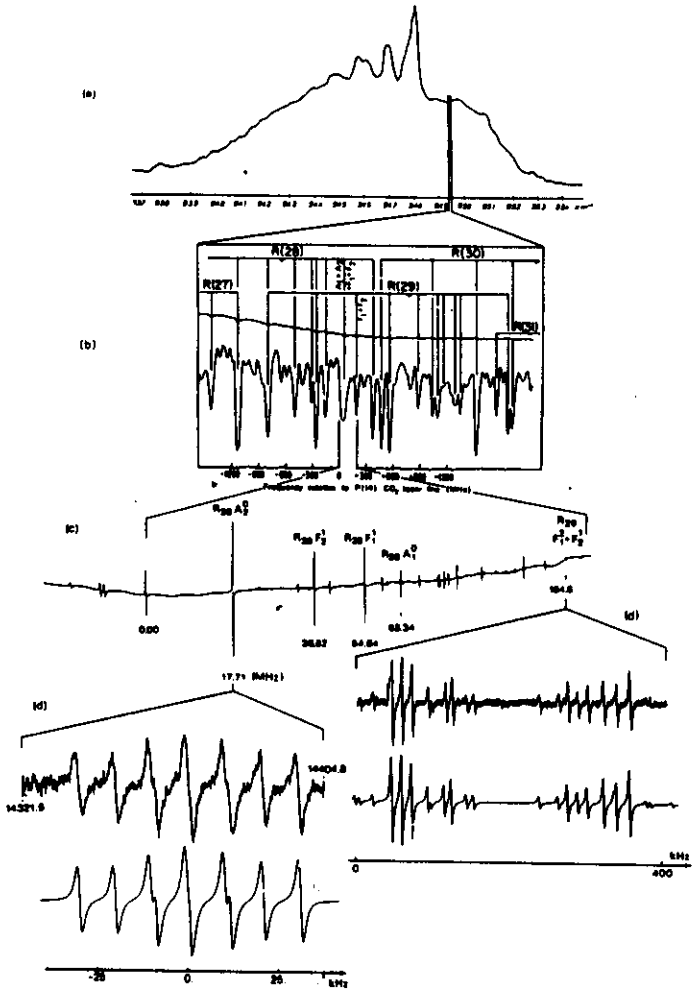

Fig. 1. Structure of the ν_3 band of $^{32}SF_6$ with increasing resolution: (a) envelope of the P, Q and R branches recorded with a conventional grating spectrometer; (b) Doppler-limited semiconductor diode laser spectrum exhibiting the tensor fine structure of J-manifolds; the superfine structure of clusters is resolved only in the saturation spectrum. (c) obtained with a free-running waveguide CO_2 laser; finally hyperfine structures are clearly resolved on saturation spectra (d) obtained with a frequency-controlled spectrometer (phase-locked waveguide CO_2 laser [3]). For comparison calculated spectra are displayed below observed structures.

FIG I - 1

now gained 6 orders of magnitude since 1969 (Fig. I-1) and in the first part of these lectures, I shall describe the 10 µm saturation spectrometer built and operated by the team led by C. Bordé at the University of Paris-North. Then I shall turn to the applications of SAS to small molecules and explain what new features are seen in the spectra ; to fully master a new technique such as SAS, it is necessary to check which new features come from the intramolecular dynamics and bring information and which features are due to the technique itself and to the particular way the molecule interacts with the electromagnetic field. The molecule chosen here is SF_6 for there has been extensive SAS studies as well as studies with other new techniques such as Doppler free two-photon spectroscopy, Infrared Infrared double resonance, stimulated Raman spectroscopy, photon echoes. Actually it has been a " pet molecule " because it absorbs CO_2 laser light and because of the interest for the laser isotope separation of UF_6. However it is only recently that the ν_3 band SF_6, which is the first step of multiphoton absorption, in known in details. In the second part of my lectures, I shall describe what we learn about the molecule when we look at it with ultra-high resolution (Fig I-1).

PART I : Experimental specifications.

I-A Description of the spectrometer.

The principle of SAS is given in Pr. Demtroder's lectures. What we need to start with are two counterpropagating laser beams to select a class of molecules with given velocity and get rid of the Doppler-broadening. Then, to do spectroscopy, one must have some tunability and some frequency calibration together with a frequency stability of the beams as high as possible ; afterwards all remaining broadening mechanisms must be minimized.

The idea of a frequency off-set locked spectrometer (Fig. I-2) was introduced by J. Hall : one reference laser is stabilized to a saturation peak and that stability is transfered to a second laser locked with a tunable frequency offset from the reference laser. Then the saturated absorption is recorded with the second laser beam which is sent into the absorption cell.

The CO_2 laser sources are mounted on a massive (16 T) vibration isolated slab (Fig I-3) on which three lasers are represented : two conventional low pressure lasers and a waveguide laser but, for current work, only two lasers are used simultaneously.

The conventional lasers are seen on Fig I-4 and were built ten years ago with a highly stable mechanical design with invar rings ; the frequency is stabilized by locking the laser on a saturation peak using a third derivative servo-loop which drives two piezo electric ceramics, a slow one which corrects slow fluctuations up to 300 Hz and a fast one. This servo system is very efficient and its only limit is the signal to noise ratio of the error signal. The spectral purity of such a laser is better than 10 Hz with slow drifts less than 25 Hz for several tens of minutes. This can be seen on the beat note of two lasers servoed independently on two saturation peaks (Fig I-5).

With these lasers and the frequency off set lock, very narrow (5 kHz) linewidths were obtained as early as 1976 ; however the disadvantage of low pressure lasers is their lack of tunability : they can be tuned only over the Dopplerwidth of the CO_2 lines ($\sim$ 60 MHz) and very few lines of few molecules could be studied. To extend the tuning range, high pressure waveguide lasers were designed and are represented on Fig I-6 . When they were first used, they were actually not locked to a conventional laser and were used as free-running lasers ; as a consequence the resolution dropped to about 40 kHz, but they were tunable over 500 MHz around each CO_2 laser line. An example of spectra recorded with the free-running waveguide laser is shown on Fig I-1 (c).

Finally the technology of these lasers was better mastered and they are now stabilized on a saturation peak with two ceramics, as a conventional laser, and, in the spectrometer, they can be locked to a conventional laser : the beat note of the two lasers is mixed to the radiofrequency of the synthetizer in a phase-lock servo-loop and, by driving the radiofrequency synthetizer,the laser is tuned over 500 MHz. Finally in the set-up we have a reference frequency given

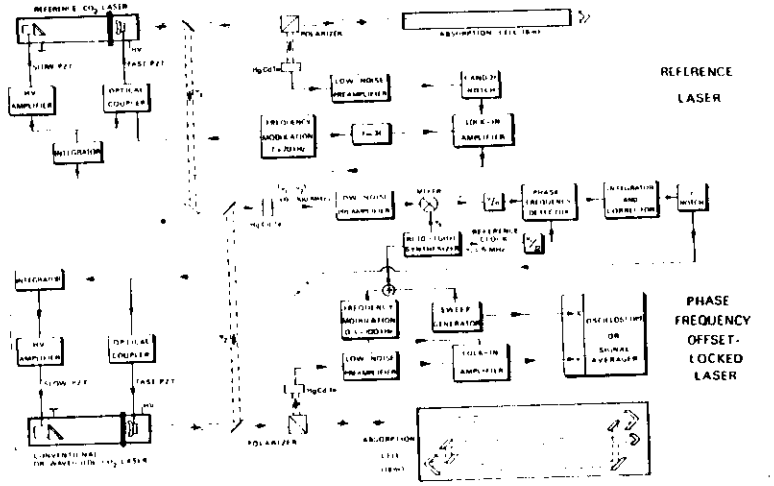

FIG I - 2

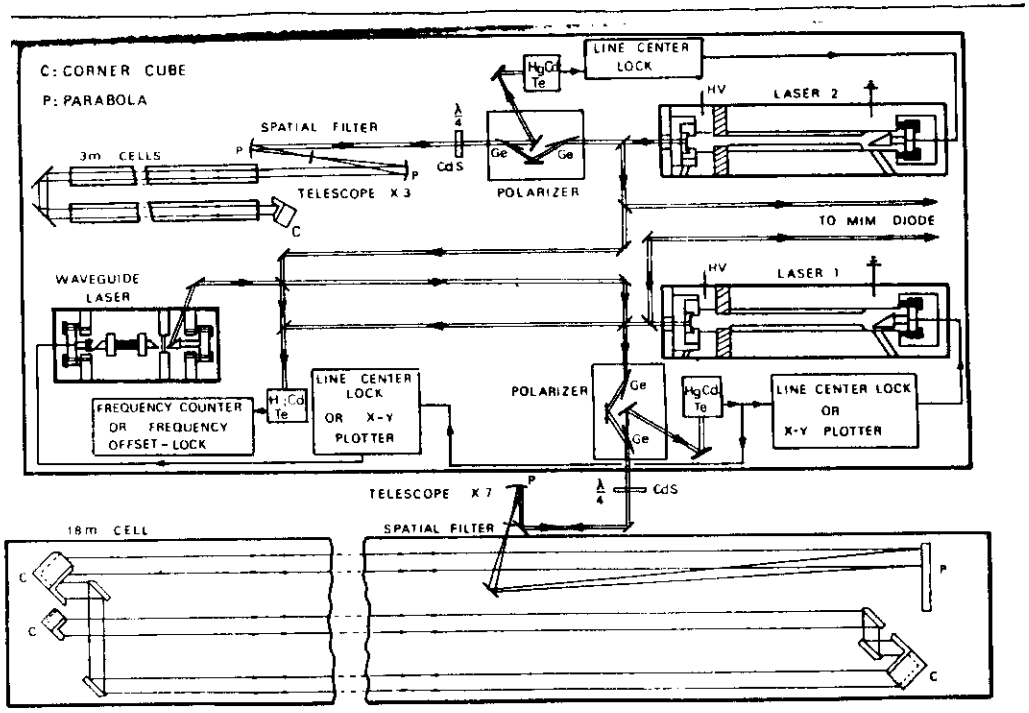

FIG I - 3

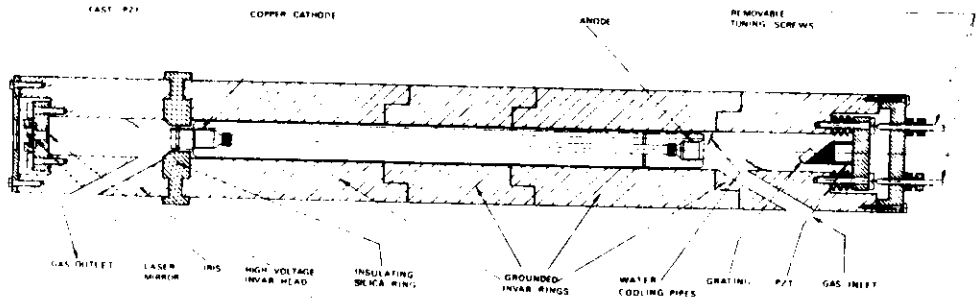

Coupe longitudinale des lasers conventionnels à basse pression : la structure tubulaire est constituée de bagues encastrées en invar supérieur et silice fondue. Seuls les embouts terminaux permettant l'accès aux composants optiques, aux électrodes et au tube laser sont démontables. Les canalisations d'eau sont raccordées à l'extérieur par passage étanche sur la face terminale du côté du réseau. Le réseau plan en acier aluminisé ou doré fonctionne en Littrow dans l'ordre – 1. La cavité oscille préférentiellement dans un plan de polarisation perpendiculaire aux sillons. L'angle de blaze ($i \sim 52°$) est compensé par une cale intermédiaire en verre. Le support du réseau peut subir des rotations autour de deux axes orthogonaux, comportant des empilements de rondelles Belleville assurant une excellente stabilité à long terme du réglage. Un iris ($\varnothing \sim 5$ mm) est indispensable pour privilégier l'oscillation du mode TEM_{00}. Le contrôle électronique de fréquence de ces lasers est assuré par deux céramiques piézoélectriques : une céramique sensible (100 kHz/V) poussant le réseau permet soit de balayer l'intervalle entre deux modes, soit d'apporter des corrections lentes alors qu'une céramique rapide située derrière le miroir de Germanium est utilisée pour la modulation de fréquence et les corrections rapides. Un coupleur optique assure l'isolement nécessaire entre la tête du laser et le système de commande de la céramique rapide.

FIG I - 4

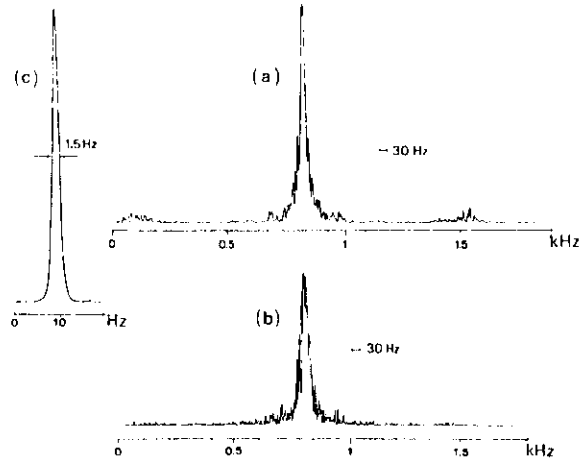

– Spectres de battement (échelles verticales linéaires) : (*a*) entre deux lasers à CO_2 conventionnels asservis sur des résonances de saturation de OsO_4 ; résolution de l'analyseur de spectre : 30 Hz; temps de balayage total : 1 minute; (*b*) mêmes conditions que (*a*), mais l'un des deux lasers conventionnels a été remplacé par un laser guide d'ondes; (*c*) le laser guide d'ondes est verrouillé en phase à un laser conventionnel ; résolution de l'analyseur de spectre : 1 Hz; temps de balayage total : 5 minutes. Le décalage électronique par boucle à verrouillage de phase assure le transfert intégral de la pureté spectrale du laser de référence ($\Gamma \sim 10$ Hz) au laser guide d'ondes accordable.

FIG I - 5

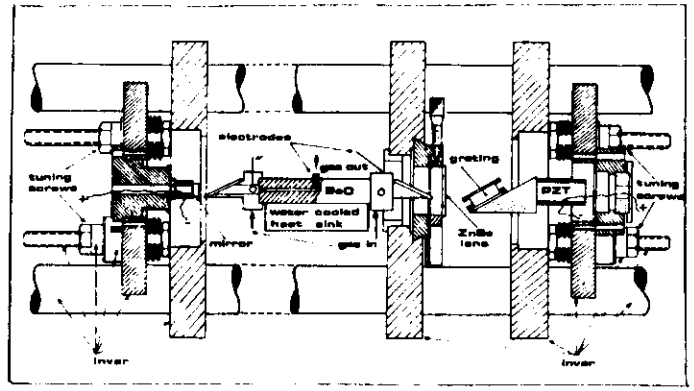

– Schéma d'un laser guide d'ondes : le tube amplificateur est construit à partir de plaques d'oxyde de beryllium polies et collées ensemble de façon à constituer un guide creux carré de 1,5 mm de côté. A chaque extrémité du guide des embouts de stéatite servent de supports aux fenêtres de Brewster en ZnSe. Le gaz (mélange 12,4 %, 14,6 %, 73 % de CO_2, N_2, He) pénètre dans le tube par ces embouts, et est pompé à travers un tube de cuivre au centre du guide. La pression moyenne dans le tube est de l'ordre de 100 Torr. Le tube de cuivre est utilisé comme cathode et deux pointes de tungstène traversant les embouts de stéatite servent d'anodes. Une alimentation stabilisée établit un courant de décharge de l'ordre de 2 mA, avec une chute de tension de l'ordre de 5 kV pour chaque demi-tube monté en série avec une résistance ballast de 1 MΩ. La chaleur est évacuée par un bloc de cuivre en contact thermique avec le guide, et refroidi par une circulation d'eau à température régulée. La cavité optique est constituée par un miroir sphérique (R = 120 mm), centré sur l'entrée du guide et un réseau (150 traits/mm) éclairé dans le premier ordre par une lentille de ZnSe ($f = 6$ cm) placée à 6 cm du guide. Deux céramiques piézoélectriques, respectivement derrière le miroir et le réseau, permettent le contrôle de fréquence du laser. La lumière est extraite dans l'ordre zéro du réseau.

FIG I - 6

by a highly stable conventional low pressure laser which is locked to a narrow saturation peak using a third derivative servo loop ; then the beat note used in the phase lock servo loop transfers completely the stability of the conventional laser to the waveguide laser.

Once we have such a nice source, we can think of the interaction between the light it emits and some system, atoms or molecules. At Villetaneuse, there are two possibilities : we can either send the beam into a cell or send it next room to interact with a supersonic molecular beam. The next step is to have a good optical quality of the laser beam whenever it interacts with the molecules. In the cell, the path of the beam is shown on Fig I-3 and to keep the optical quality of the imput beam, we use high quality corner cubes (faces polished at $\lambda/20$ and angles precise at 1") ; the radius of curvature of the wave front is about 1 kilometer with a beam waist of 4 cm. Thus the linewidth is essentially due to transit time across the wave : the finite time of interaction between the molecule and the electromagnetic field which gives a 1.2 kHz broadening. Since it is not possible to increase the transit time indefinitely (the cell is already very large : 18 meters long, 70 cm diameter), we are trying presently an other method, the Ramsey fringes technique, in which we separate the interaction into three zones, which explain the geometry shown on Fig. I-3.

I-B - Absolute frequency measurements.

We have now a good grid of frequency markers based on CO_2 lasers locked to Os O_4 saturation peaks. Os O_4 is a good candidate for that kind of metrological work for several reasons.

- as shown on Fig I-7, there are many Os O_4 lines in coincidence with each CO_2 laser line.

- Secondly, there exists an absolute frequency measurement of an Os O_4 line with an accuracy better than the kHz.

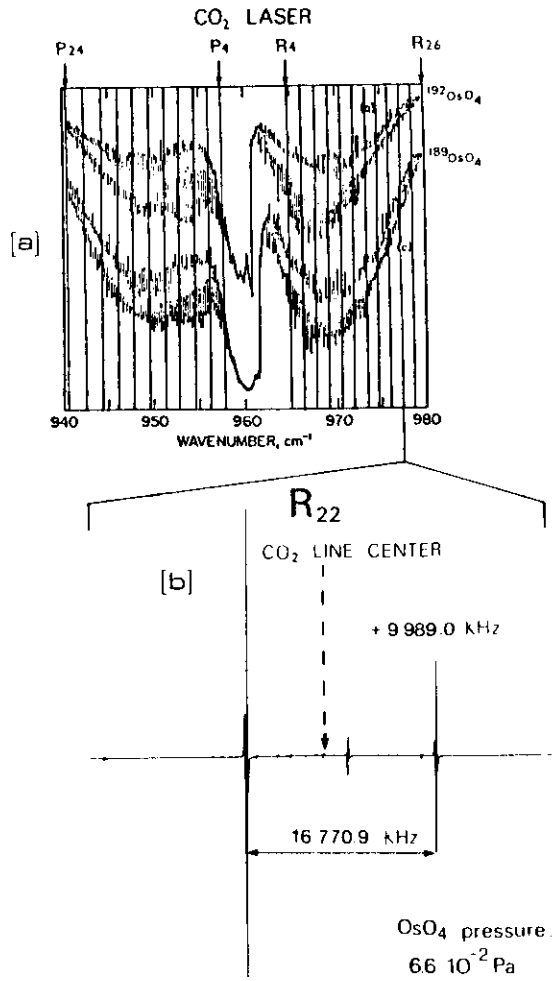

– (*a*) Bande ν_3 de deux variétés isotopiques de OsO_4 et grille de fréquences du laser à CO_2 situées à l'intérieur de cette bande. Il s'agit de spectres par transformée de Fourier tirés de la référence [52]. Les raies de $^{192}OsO_4$ sont exemptes de structure hyperfine alors que celles de $^{189}OsO_4$ ont une structure quadrupolaire bien résolue [10]. (*b*) Exemple de résonances de saturation de OsO_4 observées par détection de l'harmonique trois de la fréquence de modulation et utilisées comme raies de référence.

FIG I - 7

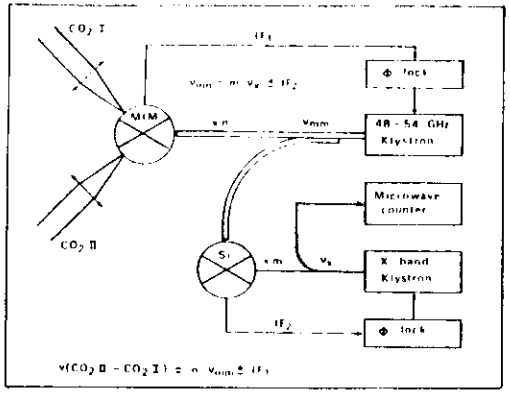

Schéma de principe du dispositif employé pour les mesures de fréquences de battement avec ses deux boucles à verrouillage de phase utilisées en conjonction avec un klystron millimétrique

FIG I - 8

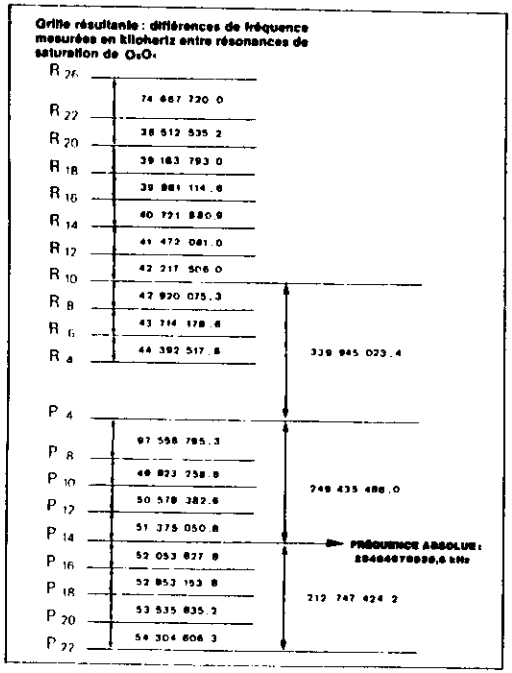

– Grille résultante des raies de référence de OsO_4 et différences de fréquence mesurées en kilohertz. La fréquence de la raie de OsO_4, en quasi-coïncidence avec la raie P(14) issue de la référence [53] permet d'attribuer une fréquence absolue à chacune des autres raies

FIG I - 9

- Finally, the lines of Os O_4 are strong and narrow because it is a heavy molecule for which the recoil splitting, the second order Doppler effect and transit effects are very small. In addition, the hyperfine structures are either completely resolved or absent.

A sketch of the method is shown in Fig I-8. Basically, a point contact MIM diode receives beams from the two stabilized CO_2 lasers and power from a Klystron. If the two laser lines are not adjacent lines, a millimeter wave Klystron is used and compared to the X band Klystron ; in that case we have two phaselock servo loops. If we have adjacent lines, only the X band Klystron is used. The recent improvement enabling one to measure non-adjacent lines allowed to reduce uncertainties, to avoid error propagation and to detect systematic errors.

So there exists now, shown on Fig I-9, a grid of frequency markers which extends over 1.12 THz and is known to 1 kHz accuracy. It is calibrated with respect to the Cesium clock and can be used for all spectroscopic work in this region and also in regions which can be reached by addition or differences of these frequencies.

PART II - Ultra high resolution spectra of SF_6

II-A - Ultimate splitings of vibration-rotation eigenvalues.

We start from the pattern of the vibration-rotation (VR) levels involved in the fundamental band of a triply degenerate vibration mode such as ν_3. In the pattern shown by Pr. Amat, each level is still highly degenerate since K and M can take 2 J + 1 values ; this degeneracy is associated with the high symmetry of the VR hamiltonian when its expansion is truncated after the first order Coriolis term : all rotations of the molecular axes and of the laboratory axes

leave the truncated hamiltonian invariant. However the true symmetry of the total VR hamiltonian H_{vr} is lower than that and the only rotations that leave H_{vr} invariant are those which leave the equilibrium configuration of SF_6 unchanged (Fig II-1). These rotations are the element of the point group O. The table of caracters of the irreducible representations (I.R.) of O is given in Table II-1. The decomposition of the representations of O spanned by the 2 J + 1 rotational functions (with different K) into I.R. of O gives the maximum possibility of splitting to expect for the 2 J + 1 eigenvalues of H_{vr}. The formula which tells how many times each I.R. of O appears for a given value of J is given in Table II-2 ; since the same type appears several times, an additional counting index n is necessary to distinguish identical I.R. The eigenvalues of H_{vr} will then be labeled JC^n in the ground state (C = A_1, A_2, E, F_1, F_2). In the v_3 = 1 state, we have similar considerations but J must be replaced by R and an eigenvalue of H_{vr} will finally be labeled by J R C^n (with R = J in v_3 = 0 and R = J, J ± 1 in v_3 = 1).

The next question is "do we reach this maximum decomposition of JR levels?". The answer is yes : there are indeed operators in the expansion of H_{vr} which produce this splitting (Table II-3). In a carefully chosen basis of wavefunctions labeled by the I.R. (JRC^n), we find operators which are diagonal in this basis but which have different matrix elements for different C or n, The main operators to do that are called T_{044} and T_{224} and represent contributions to the centrifugal distortion and to the vibrational dependence of B. The splittings, according to the values of C^n are described by a factor F (R, nC) in the matrix elements (see Table II-4) and these factors have been tabulated (see examples in Table II-5 for R = 39 and 88). What can be seen from Table II-5 is that these splittings are far from being equal but, on the contrary, the split eigenvalues are gathered into clusters. This clustering has been described at length in the literature and its physical reasons are related to the fact that, at one end of the R manifold, the molecule is rotating around a threefold axis while, at the other end, it is rotating around of fourfold axis .There are six equivalent fourfold axes leading to a near degeneracy of six states and eight equivalent threefold axes leading to near degeneracy of eight states. The

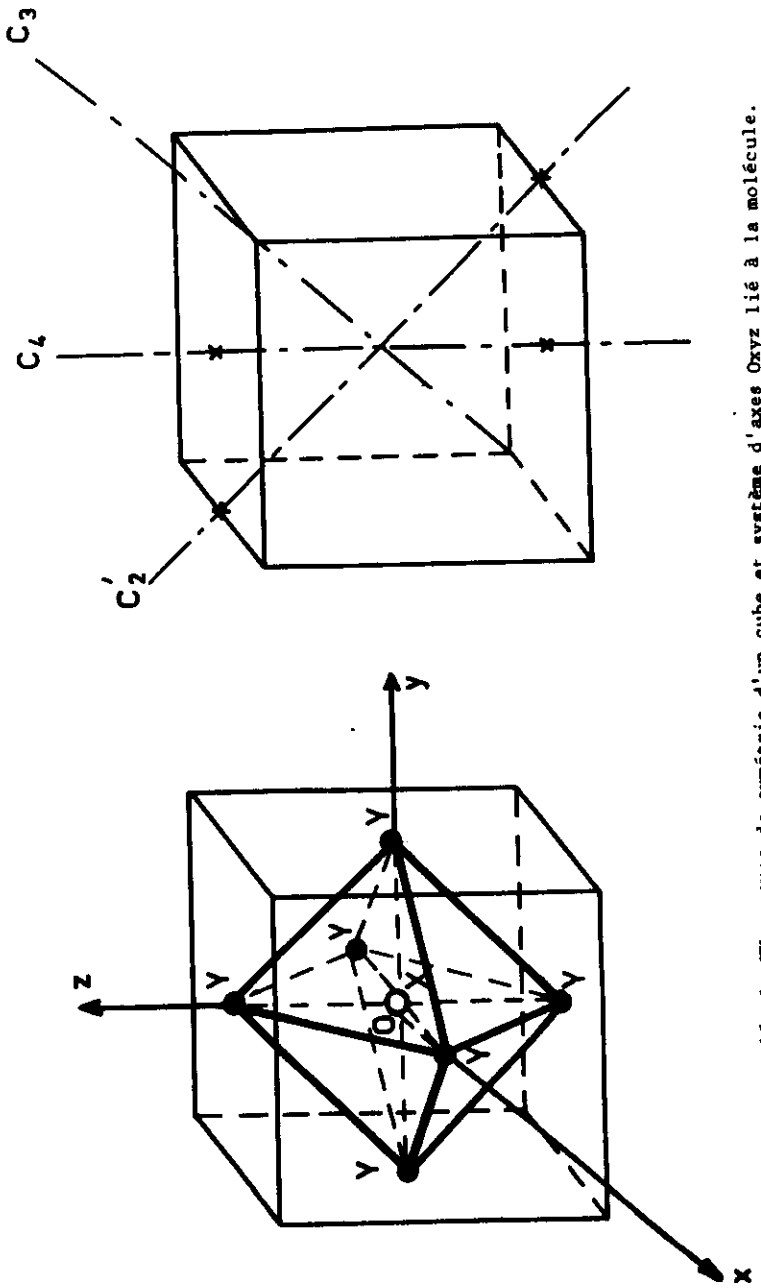

- Molécule XY_6 , axes de symétrie d'un cube et système d'axes Oxyz lié à la molécule.

FIG II - 1

TABLE DE CARACTERES DES GROUPES T_d ET O

O		$\mathcal{E}$	$C_3(8)$	$C_4^2(3)$	$C_2(6)$	$C_4(6)$	Types de symétrie de certaines coordonnées
	T_d	$\mathcal{E}$	$C_3(8)$	$C_2(3)$	$\sigma_d(6)$	$S_4(6)$	de T_d
A1	A1	1	1	1	1	1	Q_1
A2	A2	1	1	1	-1	-1	
E	E	2	-1	2	0	0	$Q_{2\alpha}$
F2	F2	3	0	-1	1	-1	$T_\alpha; O_{3\alpha}; O_{4\alpha}$
F1	F1	3	0	-1	1	1	R_α

TABLE II - 1

J	$\mathcal{D}_g^{(J)}$
12p	p(A1 + A2 + 2E + 3F1 + 3F2) + A1
12p + 1	p(A1 + A2 + 2E + 3F1 + 3F2) + F1
12p + 2	p(A1 + A2 + 2E + 3F1 + 3F2) + E + F2
12p + 3	p(A1 + A2 + 2E + 3F1 + 3F2) + A2 + F1 + F2
12p + 4	p(A1 + A2 + 2E + 3F1 + 3F2) + A1 + E + F1 + F2
12p + 5	p(A1 + A2 + 2E + 3F1 + 3F2) + E + 2F1 + F2
12p + 6	p(A1 + A2 + 2E + 3F1 + 3F2) + A1 + A2 + E + F1 + 2F2
12p + 7	p(A1 + A2 + 2E + 3F1 + 3F2) + A2 + E + 2F1 + 2F2
12p + 8	p(A1 + A2 + 2E + 3F1 + 3F2) + A1 + 2E + 2F1 + 2F2
12p + 9	p(A1 + A2 + 2E + 3F1 + 3F2) + A1 + A2 + E + 3F1 + 2F2
12p + 10	p(A1 + A2 + 2E + 3F1 + 3F2) + A1 + A2 + 2E + 2F1 + 3F2
12p + 11	p(A1 + A2 + 2E + 3F1 + 3F2) + A2 + 2E + 3F1 + 3F2

TABLE II - 2

VIBRATION-ROTATION HAMILTONIAN FOR A TRIPLY DEGENERATE MODE (ν_3)

$$H = \tfrac{1}{2}\omega_3\left(P_3^2 + q_3^2\right) + X_{33}\left[\tfrac{1}{2}(P_3^2+q_3^2)\right]^2 + G_{33}\,\ell_3^2 + T_{33}O_{33} + \cdots$$

Harmonic Oscillator — Scalar Anharmonicity — Tensor Anharmonicity

$$+ BJ^2 - 2B\zeta_3\,\vec{J}\cdot\vec{\ell}_3 - D_s\left(\vec{J}^2\right)^2 + \cdots$$

Rigid Rotor — Coriolis Interaction — Scalar Centrifugal Distortion

$$- D_t\left[10\left(J_x^4 + J_y^4 + J_z^4\right) - 6\left(J^2\right)^2 + 2J^2\right] + t_{224}\,T_{224} + \cdots$$

Tensor Centrifugal Distortion — Tensor vibrational dependence of B

TABLE II - 3

O	O_h	Total nuclear spin
A_1	A_{1g}	I = 0
	A_{1u}	I = 0
A_2	A_{2u}	I = 1,3
E	E_u	I = 1,2
F_1	F_{1g}	I = 1
	F_{1u}	I = 1
F_2	F_{2g}	I = 0,2

Symmetry species of

Correspondence between I and C in SF_6

TABLE II - 6

F (R,C,n)

J = 39

	Fa
F1(0)	7,5709503411131926086533766920-02
F2(0)	7,5[illegible]331[illegible]5[illegible]5378560-02
A2(0)	5,[illegible]1[illegible]3[illegible]3[illegible]1[illegible]-02
F1(1)	5,[illegible]2744[illegible]0[illegible]-02
E (0)	5,8304125115527350[illegible]3[illegible]1120-02
F1(1)	3,9180347[illegible]0[illegible]2[illegible]0[illegible]-02
F2(2)	3,9180241[illegible]2[illegible]1[illegible]0[illegible]-02
E (1)	2,4212[illegible]0[illegible]2[illegible]0[illegible]-02
F1(2)	2,4211[illegible]0[illegible]2[illegible]0[illegible]-02
A1(0)	2,4210[illegible]0[illegible]0[illegible]0[illegible]-02
F1(3)	1,1294[illegible]0[illegible]0[illegible]0[illegible]-02
F2(3)	1,1271[illegible]2[illegible]0[illegible]0[illegible]-02
A2(1)	3,9157[illegible]2[illegible]0[illegible]0[illegible]-04
F2(4)	3,[illegible]0[illegible]0[illegible]0[illegible]-04
E (2)	2,5[illegible]0[illegible]0[illegible]0[illegible]-04
F1(4)	-8,5[illegible]0[illegible]0[illegible]0[illegible]-03
F2(5)	-8,[illegible]0[illegible]0[illegible]0[illegible]-03
E (3)	-1,[illegible]0[illegible]0[illegible]0[illegible]-02
F1(5)	-1,[illegible]0[illegible]0[illegible]0[illegible]-02
A1(1)	-1,7[illegible]0[illegible]0[illegible]0[illegible]-02
F1(6)	-2,[illegible]0[illegible]0[illegible]0[illegible]-02
F2(6)	-2,[illegible]0[illegible]0[illegible]0[illegible]-02
A2(2)	-2,3[illegible]0[illegible]0[illegible]0[illegible]-02
F2(7)	-2,[illegible]0[illegible]0[illegible]0[illegible]-02
E (4)	-2,[illegible]0[illegible]0[illegible]0[illegible]-02
F1(7)	-2,9[illegible]0[illegible]0[illegible]0[illegible]-02
F2(8)	-3,[illegible]0[illegible]0[illegible]0[illegible]-02
E (5)	-3,[illegible]0[illegible]0[illegible]0[illegible]-02
F1(8)	-3,[illegible]0[illegible]0[illegible]0[illegible]-02
A1(2)	-5,[illegible]0[illegible]0[illegible]0[illegible]-02
F1(9)	-5,0[illegible]0[illegible]0[illegible]0[illegible]-02
F2(9)	-5,[illegible]0[illegible]0[illegible]0[illegible]-02
A2(3)	-5,[illegible]0[illegible]0[illegible]0[illegible]-02

TABLE II - 5

J = 40

	Fa
A1(7)	5,[illegible]0[illegible]0[illegible]0[illegible]-02
F1(21)	5,[illegible]0[illegible]0[illegible]0[illegible]-02
E (14)	5,[illegible]0[illegible]0[illegible]0[illegible]-02
F2(23)	[illegible]0[illegible]0[illegible]0[illegible]-02
F1(20)	[illegible]0[illegible]0[illegible]0[illegible]-02
E (13)	[illegible]0[illegible]0[illegible]0[illegible]-02
F2(20)	[illegible]0[illegible]0[illegible]0[illegible]-02
A2(6)	[illegible]0[illegible]0[illegible]0[illegible]-02
F2(19)	[illegible]0[illegible]0[illegible]0[illegible]-02
F1(19)	[illegible]0[illegible]0[illegible]0[illegible]-02
A1(6)	[illegible]0[illegible]0[illegible]0[illegible]-02
F1(18)	[illegible]0[illegible]0[illegible]0[illegible]-02
E (12)	[illegible]0[illegible]0[illegible]0[illegible]-02
F2(18)	[illegible]0[illegible]0[illegible]0[illegible]-02
F1(17)	[illegible]0[illegible]0[illegible]0[illegible]-02
E (11)	[illegible]0[illegible]0[illegible]0[illegible]-02
F2(17)	[illegible]0[illegible]0[illegible]0[illegible]-02
A2(5)	[illegible]0[illegible]0[illegible]0[illegible]-02
F2(16)	[illegible]0[illegible]0[illegible]0[illegible]-02
F1(16)	[illegible]0[illegible]0[illegible]0[illegible]-02
A1(5)	[illegible]0[illegible]0[illegible]0[illegible]-02
F1(15)	[illegible]0[illegible]0[illegible]0[illegible]-02
E (10)	[illegible]0[illegible]0[illegible]0[illegible]-02
F2(15)	[illegible]0[illegible]0[illegible]0[illegible]-03
F1(14)	[illegible]0[illegible]0[illegible]0[illegible]-03
E (9)	[illegible]0[illegible]0[illegible]0[illegible]-03
A2(14)	[illegible]0[illegible]0[illegible]0[illegible]-03
A2(4)	[illegible]0[illegible]0[illegible]0[illegible]-03
F2(13)	[illegible]0[illegible]0[illegible]0[illegible]-03
F1(13)	[illegible]0[illegible]0[illegible]0[illegible]-03
A1(4)	[illegible]0[illegible]0[illegible]0[illegible]-04
F1(12)	[illegible]0[illegible]0[illegible]0[illegible]-04
E (8)	[illegible]0[illegible]0[illegible]0[illegible]-04
F2(12)	[illegible]0[illegible]0[illegible]0[illegible]-03
F1(11)	[illegible]0[illegible]0[illegible]0[illegible]-03
E (7)	[illegible]0[illegible]0[illegible]0[illegible]-03
F2(11)	[illegible]0[illegible]0[illegible]0[illegible]-03
A2(3)	[illegible]0[illegible]0[illegible]0[illegible]-03
F2(10)	[illegible]0[illegible]0[illegible]0[illegible]-03
F1(10)	[illegible]0[illegible]0[illegible]0[illegible]-03
A1(3)	[illegible]0[illegible]0[illegible]0[illegible]-02
F1(9)	[illegible]0[illegible]0[illegible]0[illegible]-02
E (6)	[illegible]0[illegible]0[illegible]0[illegible]-02
F2(9)	[illegible]0[illegible]0[illegible]0[illegible]-02
F1(8)	[illegible]0[illegible]0[illegible]0[illegible]-02
E (5)	[illegible]0[illegible]0[illegible]0[illegible]-02
F2(8)	[illegible]0[illegible]0[illegible]0[illegible]-02
A2(2)	[illegible]0[illegible]0[illegible]0[illegible]-02
F2(7)	[illegible]0[illegible]0[illegible]0[illegible]-02
F1(7)	[illegible]0[illegible]0[illegible]0[illegible]-02
A1(2)	[illegible]0[illegible]0[illegible]0[illegible]-02
F1(6)	[illegible]0[illegible]0[illegible]0[illegible]-02
E (4)	[illegible]0[illegible]0[illegible]0[illegible]-02
F2(6)	[illegible]0[illegible]0[illegible]0[illegible]-02
A2(1)	[illegible]0[illegible]0[illegible]0[illegible]-02
F2(5)	[illegible]0[illegible]0[illegible]0[illegible]-02
F1(5)	[illegible]0[illegible]0[illegible]0[illegible]-02
E (3)	[illegible]0[illegible]0[illegible]0[illegible]-02
F2(5)	[illegible]0[illegible]0[illegible]0[illegible]-02
A2(1)	[illegible]0[illegible]0[illegible]0[illegible]-02
F2(4)	[illegible]0[illegible]0[illegible]0[illegible]-02
F1(4)	[illegible]0[illegible]0[illegible]0[illegible]-02
A1(1)	[illegible]0[illegible]0[illegible]0[illegible]-02
F1(3)	[illegible]0[illegible]0[illegible]0[illegible]-02
E (2)	[illegible]0[illegible]0[illegible]0[illegible]-02
F2(3)	[illegible]0[illegible]0[illegible]0[illegible]-02
F1(2)	[illegible]0[illegible]0[illegible]0[illegible]-02
E (1)	[illegible]0[illegible]0[illegible]0[illegible]-02
F2(2)	[illegible]0[illegible]0[illegible]0[illegible]-02
A2(0)	[illegible]0[illegible]0[illegible]0[illegible]-02
F2(1)	[illegible]0[illegible]0[illegible]0[illegible]-02
F1(1)	[illegible]0[illegible]0[illegible]0[illegible]-02
A1(0)	[illegible]0[illegible]0[illegible]0[illegible]-02
F1(0)	[illegible]0[illegible]0[illegible]0[illegible]-02
E (0)	[illegible]0[illegible]0[illegible]0[illegible]-02
F2(0)	[illegible]0[illegible]0[illegible]0[illegible]-02

TENSORIAL DECOMPOSITION OF (J, R, ν_3) STATES

STATE	OPERATOR	CONSTANT	MATRIX ELEMENT
$\nu_3 = 0$	T_{044}	$t_{044} = 5.7$ kHz,	$t_{044}\ f(J,R)\ F(R,nC)$
$\nu_3 = 1$	T_{114} & T_{044}	$t_{114} = 1126$ kHz, $\simeq t_{114}\ \frac{f(J,R)}{R^2}\ F(R,nC)$	

F(R, nC) IS RESPONSIBLE FOR THE CLUSTERIZATION OF (J, R, ν_3) STATES

SPLITTINGS WITHIN CLUSTERS IN $\nu_3 = 1 \simeq$ SUPERFINE STRUCTURE

TABLE II - 4

splittings within a cluster are called superfine splittings and can be extremely small, especially for high R values and towards the ends of the R-manifolds. The clustering is quite similar in $v_3 = 0$ and in $v_3 = 1$ but there is an important scaling factor because $t_{044} << t_{224}$ (see Table II-4) and because the matrix elements of T_{224} are zero in $v_3 = 0$. Actually the tensor centrifugal distortion constant t_{044} has been determined by us from hyperfine structures and could not be determined before from the fit of VR lines ; the splittings of lines in the VR spectra reflect almost exactly the splittings of the $v_3 = 1$ levels. The superfine splittings of lines have been resolved with SAS (see Fig. I-1).

II-B - Hyperfine interactions.

If we look now at still higher resolution we see that even a line with a given C^n such as the R 28 A_2^o line of Fig I-1 is further split. To understand these splittings, it is necessary to invoke terms which are not in the expansion of H_{vr} and which involve the nuclear spins. In the point group O, we can find nuclear spin functions which are symmetry-adapted and have definite symmetry species C and this help finding the nuclear statistical weights which are important for the intensities of VR lines as mentioned by Pr. Amat. We can associate several nuclear spin wavefunctions with the same VR wavefunction provided the Pauli principle is satisfied; then the different total wavefunctions have the same energy since no term involves the nuclear spin in H_{vr}.

If now we add, to H_{vr}, operators which act on the nuclear spin wave - functions, VR levels will be split. A simple example of such an operator is the dot product I.J, where I is the total nuclear spin of the six fluorine, which will split VR levels into 2I + 1 sublevels labeled by the quantum number F (F = I + J) . This interaction called the scalar spin-rotation interaction is what we see in Fig I-1 (d) since, for and A_2VR level the total nuclear spin I can take the values 1 and 3. The correspondence between the symmetry species of the VR level and the possible values of I is given in the Table II-6. Let us see now more closely the operators involving the nuclear spins.

II-B-1 - Spin-rotation interaction (Table II-7)

The magnetic field created by the rotation of the molecular charges (electrons and nuclei) at the site of a nucleus interacts with the spin of that nucleus. It is related to the angular momentum J through the tensor C^i which is diagonal and involves only two constants $C_\perp$ and $C_{//}$ (for symmetry reasons) which are related to the usual coupling constants c_a and c_d. There is a very similar interaction due to the vibrational angular momentum l_3 (which has no effect if $l_3 = 0$) and which has the same expression (l_3 replaces J) but two different coupling constants.

II-B-2 - Spin-spin interaction (Table II-8).

If we start from the classical expression of the interaction between two magnetic dipoles, we obtain the direct spin-spin hamiltonian by expressing the nuclear magnetic dipole as a function of the nuclear spin. In a first approximation, we can take for the internuclear distances r_{ij}, the values at the equilibrium configuration ; there are two distances in SF_6, between adjacent nuclei and between opposite nuclei, which give two constants ; up to now I have not introduced any variation of these two parameters with the molecular state.

II-B-3 - Symmetry-adapted expression (Table II-9)

In order to calculate easily the matrix elements of these operators and, in particular, to see more conveniently which matrix elements may

Two spin-rotation hamiltonians

$$W^{k}_{SR} = -\mu^{k}\cdot B^{k} = -g_I\beta_N I^{k}\cdot B^{k} = -hI^{k}\cdot C^{k}J\,,$$

$$C^{1}(\mathrm{MFF}) = C^{0}(\mathrm{MFF}) = \begin{pmatrix} C_\perp & 0 & 0 \\ 0 & C_\perp & 0 \\ 0 & 0 & C_\parallel \end{pmatrix},$$

$$C^{k}(\mathrm{MFF}) = c_s I + \tfrac{1}{3}c_d\,\epsilon^{k}(\mathrm{MFF}), \qquad \epsilon^{1}(\mathrm{MFF}) = \epsilon^{0}(\mathrm{MFF}) = \begin{pmatrix} 1 & 0 & 0 \\ 0 & 1 & 0 \\ 0 & 0 & -2 \end{pmatrix}$$

$$W^{S}_{SR} = -hc_s\sum_k I^{k}\cdot J\,, \qquad W^{T}_{SR} = -\tfrac{1}{3}hc_d\sum_k I^{k}\epsilon^{k}(\mathrm{SFF})J$$

TABLE II - 7

The direct spin-spin hamiltonian

$$W^{ij}_{SS} = \mu^{i}\cdot\mu^{j}/|r_{ij}|^{3} - 3(r_{ij}\cdot\mu^{i})(r_{ij}\cdot\mu^{j})/|r_{ij}|^{5}\,,$$

$$\mu^{i} = g_I\beta_N I^{i}, \qquad d_1 = g_I^{2}\beta_N^{2}/R^{3}, \quad d_2 = d_1/2\sqrt{2}\,.$$

$$W^{ij}_{SS} = -(\sqrt{6}/|r_{ij}|^{3})\sum_{\mu}(-1)^{\mu}C^{(2)ij}_{-\mu}(\mathrm{SFF})[\mu^{i}\times\mu^{j}]^{(2)}_{\mu}\,,$$

$$W_{SS} = \sum_{i<j} W^{ij}_{SS}$$

TABLE II - 8

MAGNETIC HYPERFINE INTERACTIONS

NAME	OPERATOR	CONSTANT
SCALAR SPIN ROTATION $I_1 + I_2 + \ldots + I_6$	$I.J = \left[\mathcal{O}^{(A_1)}_{NS} \otimes \mathcal{O}^{(A_1)}_{VR}\right]^{(A_1)}$	$c_s\,,\ c_{s_2}$
TENSOR SPIN ROTATION	$\left[\mathcal{O}^{(E)}_{NS} \otimes \mathcal{O}^{(E)}_{VR}\right]^{(A_1)}$	$c_d\,,\ c_{d_2}$
SPIN SPIN	$\left[\mathcal{O}^{(F_2)}_{NS} \otimes \mathcal{O}^{(F_2)}_{VR}\right]^{(A_1)}$ $\left[\mathcal{O}^{(E)}_{NS} \otimes \mathcal{O}^{(E)}_{VR}\right]^{(A_1)}$	$d_1\ ;\ d_2$
SCALAR SPIN VIBRATION	$I.\ell = \left[\mathcal{O}^{(A_1)}_{NS} \otimes \mathcal{O}^{(A_1)}_{VR}\right]^{(A_1)}$	A
TENSOR SPIN VIBRATION	$\left[\mathcal{O}^{(E)}_{NS} \otimes \mathcal{O}^{(E)}_{VR}\right]^{(A_1)}$	A_2

$\langle \Psi^{C}_{VR} | H | \Psi^{C'}_{VR} \rangle \neq 0$ if C and C' = E or F_2 or A_1

TABLE II - 10

$$\ldots O(3)\times O_{NS}(3) \supset \ldots O(3)\times G \qquad (J_{z_3}, G)$$

$$(J, M, R_T, C_R, v_3, \alpha), \qquad (I_z, M_I, C_S, \alpha),$$

$$(J_z I_z)M_T, (R_T, C_R C_S)A_{2u}; v_3, \alpha),$$

$$[\mathcal{A}^{(J_z,G)}_{VR} \times H^{(I_z,G)}_{NS}]^{(0,A_{1g})}.$$

$$(JI)FM_F(R_T, C_R C_S)A_{2u}; v_3, \alpha)[H^{(J',G')}_{VR} \times H^{(I',G')}_{NS}]^{(0,A_{1g})}[J'I']F'M_F(R'_T C'_R C'_S)A_{2u}; v_3, \alpha)$$

$$= \delta_{FF'}\delta_{M_F M_F'}\frac{(-1)^{A_{2u}+G'+C_R+C_S+J''+I+J'}}{[G']^{1/2}[J''+1]^{1/2}}\begin{Bmatrix} G'_R & G'_S & I_{2u} \\ G_S & G_R & G'' \end{Bmatrix}\begin{Bmatrix} J' & J'' & F \\ J & I & J'' \end{Bmatrix}$$

$$\times (J, R_T C_R v_3 \alpha | H^{(J'',G'')}_{VR} | J', R'_T C'_R v'_3 \alpha')(I, C_S \| H^{(I'',G'')}_{NS} \| I' C'_S).$$

Symmetry-adapted notations

TABLE II - 9

$$W^{S}_{SR} = hc_s\sqrt{3}\left[I^{(1,A_{1g})} \times \left[D^{(1,1)} \times \ell^{(0,1)}\right]^{(1,\sigma A_{1g})}\right]^{(0,A_{1g})} = -hc_s\, I.J$$

$$W^{T}_{SR} = -hc_d\,[I^{(1,F_g)} \times [D^{(2,2)} \times J^{(1,0)}]^{(1,2E_g)}]^{(0,A_{1g})}.$$

$$W^{S}_{SS} = -3h\,[D^{(2,2E_g)} \times \{(d_1+d_2)[I\times I]^{(2,E_g)} + (d_1-d_2)[I\times I]^{(2,E'_g)}\}]^{(0,A_{1g})}$$
$$-3\sqrt{6}hd_1\,[D^{(2,2F_{2g})} \times [I\times I]^{(2,F_{2g})}]^{(0,A_{1g})},$$

$$W^{S}_{SV} = -hA\sqrt{3}\,[I^{(1,A_{1g})} \times [D^{(1,1)} \times I_3^{(0,1)}]^{(1,\sigma A_{1g})}]^{(0,A_{1g})} = hA\,I_3\,I_3\,,$$

$$W^{T}_{SV} = hA[I^{(1,F_g)} \times [D^{(1,1)} \times I_3^{(0,1)}]^{(1,2E_g)}]^{(0,A_{1g})},$$

Symmetry-adapted hyperfine hamiltonians

not vanish, we transform the expressions to symmetry-adapted expressions in the symmetry group of the Hamiltonian. We extend somewhat the point group and choose to use $^{L}O(3) \times O_h$ where $^{I}O(3)$ is the orthogonal group of the laboratory-fixed axes and where x denotes the direct product of two groups. This group is appropriate because it is easier to deal with the vibration-rotation in the molecule-fixed axes while the nuclear spin are better handled in the laboratory-fixed axes ; so we want to keep track of the behaviour of the operators and wavefunctions in both groups. The V.R. operators and wavefunction and nuclear spin operators and functions are separately symmetry-adapted and are then coupled with the requirements that the total wavefunction satisfies the Pauli principle and that the hamiltonian is totally symmetric. What we have gained is that we can use the full power of Racah algebra to calculate the matrix elements, both the usual Racah algebra in $^{L}O(3)$, but also its equivalent in the point group O_h with 6-C symbols analogous to the 6-j symbols. The key point when we look at these operators is to realize that they involve VR operators which are not A_{1g} so that, now, VR states with different species C in O_h can mix.

II-B-4 Hyperfine induced crossovers.

Among the coupling constants, only d_1, d_2 and c_a were known in 1977 and in particular c_d and t_{044} which are so important for the ground state pattern of levels were unknown ; fortunately, SAS provided us with some spectral features which are specific to SAS and which gave access to the ground state ; in addition to the usual lines that one expects from linear absorption spectroscopy, the technique of saturation spectroscopy provides us with an extra line each time two transitions share a common level, either upper or lower level (Fig II-2). These lines are called crossovers and are located halfway between the two parent lines ; their intensities are the geometrical means of the two parent intensities. What happens then is illustrated on Fig II-3 in the case of a doublet : the hyperfine interactions break the selection rule $\Delta C = 0$ since C and C' VR

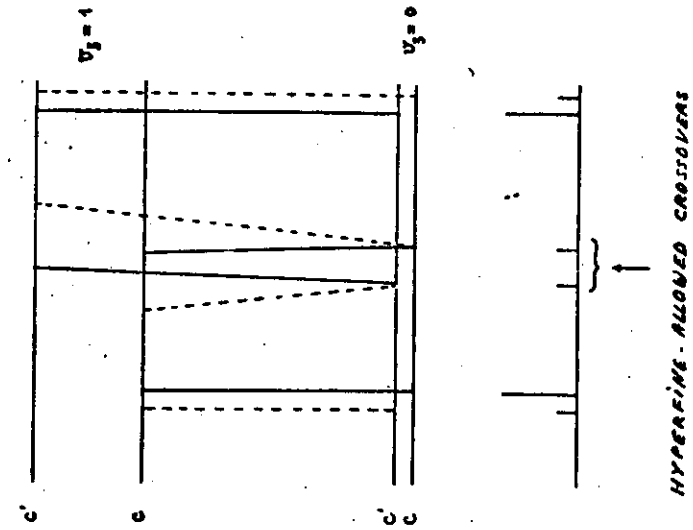

FIG II - 3

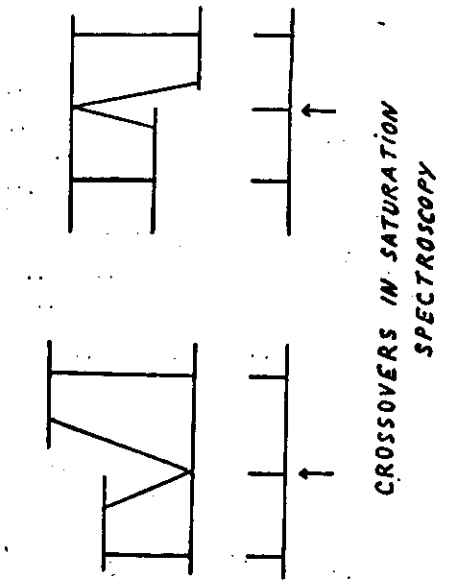

FIG II - 2

states are mixed and crossovers with lower common levels appear between the main lines. The real situation in the coupled basis is drawn on Fig II-4 with the hyperfine sublevels. The structure of these crossovers enables one to determine the constants responsible for this pattern of sublevels in the ground state namely t_{044} and $|c_d|$. The triplet Q(38) F_1° E° F_2° is an other example of the same phenomenon (Fig II-5) in which, the necessity to indroduce the overal parity, g or u, is clearly seen.

II-B-5 - Hyperfine structures of lines.

These spectral structures can look very different from one another because the pattern of levels can be very different both in $v_3 = 0$ and in $v_3 = 1$ states ; we can distinguish three cases :

a) in both vibrational states, the VR splittings of neighbour states are large enough compared to off-diagonal hyperfine matrix elements.

b) the VR splittings are large enough only in the $v_3 = 1$ state .

c) the VR splittings are small is both states.

In case a) the hyperfine structures are pretty regular and it is easy to recognize the hyperfine components according to the possible values of the total angular momentum and the total nuclear spin. Such an example is R28 A_2° shown in Fig I-1 (d). Other example for other symmetry species of O have been observed.

In cases (b) which are the most frequent cases, given the small value of t_{044}, VR states are strongly mixed in $v_3 = 0$ and, though the VR lines look isolated, because VR splittings are large in $v_3 = 1$, the hyperfine structure of these lines are fairly perturbed. The triplet Q 52 A^2 F_1^6 E^4 is such an example (Fig II-6).

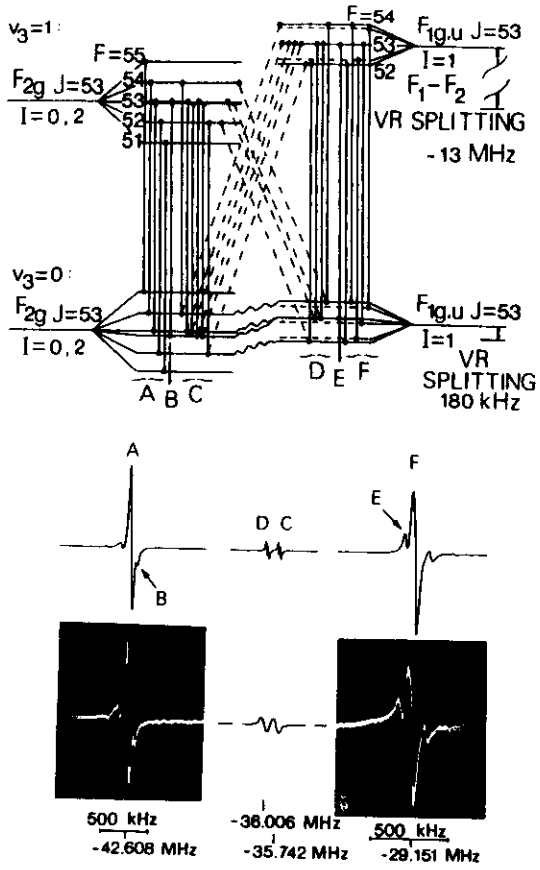

FIG II - 4

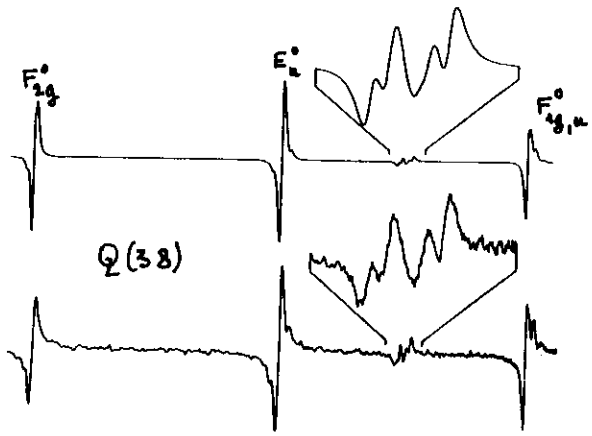

FIG II - 5

Finally, in an extreme case (c), the VR splittings can be zero in both vibrational states and this is called a superhyperfine structure. Tetragonal superhyperfine structures are suprisingly very regular, exhibiting equidistant quadruplets of hyperfine components and these patterns can be explained physically with a simple model. A superhyperfine F_1 F_2 cases is shown on Fig II-7 : however as soon as the VR splitting is not exactly zero, this nice regularity is lost and the hyperfine structures become more complicated. Many hyperfine structures have been observed in the PQ and R branches of the ν_3 band, belonging to cases a, b and c or being intermediate between cases (sec R29 F_1^2 , F_2^1 on Fig. I-1). Despite the variety of patterns they have all been fitted with synthetic spectra using the theoretical model described in II B1 and II B2 and, from this fit we have been able, to determine accurate values of the coupling constants.

Most of the material and Figures of these lectures was taken from the following references :

1) C. Bordé Revue du Cethedec - Ondes et signal NS 83-1, 1983 (in French, available on request).

2) J. Bordé and C. Bordé Chemical Physics 71, 417 (1982), 84, 159 (1984)

3) A. Van Lerberghe, S. Avrillier , C. Bordé I.E.E.E. J. Quantum Electr. QE14, 481 (1978).

4) Ch. Salomon, Ch. Bréant, A.Van Lerberghe, G. Camy, C. Bordé Applied Physics. B, 29, 153 (1982).

5) A. Clairon, A. Van Lerberghe, Ch Bréant, Ch. Salomon, G. Camy, C. Bordé J. Phys (Paris), 42, Supplement to n° 12, p C8-127 (1981).

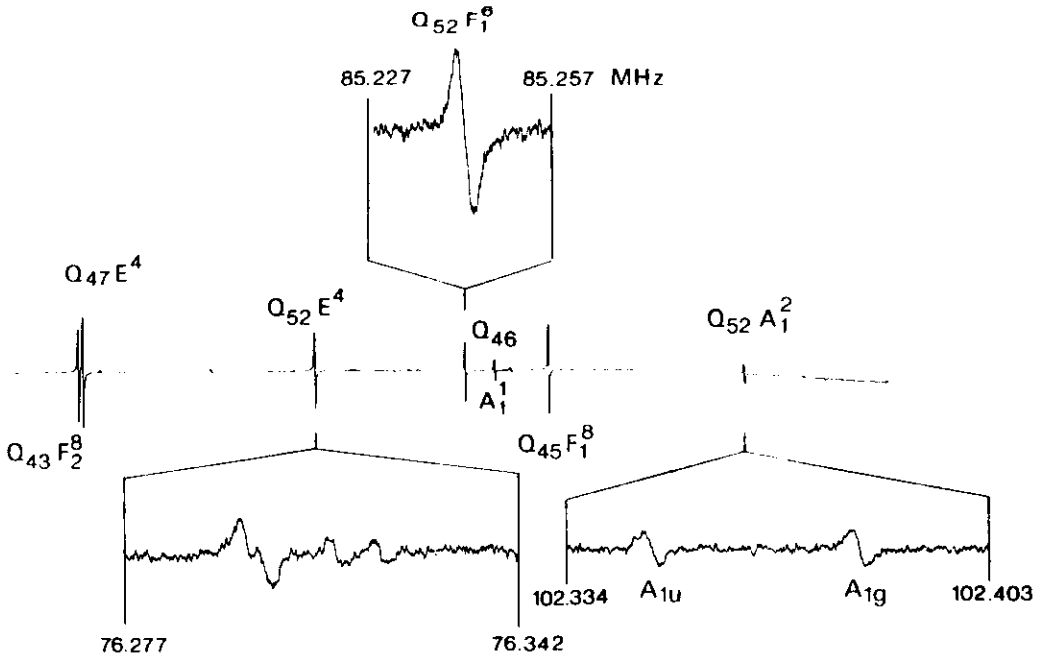

FIG II - 6

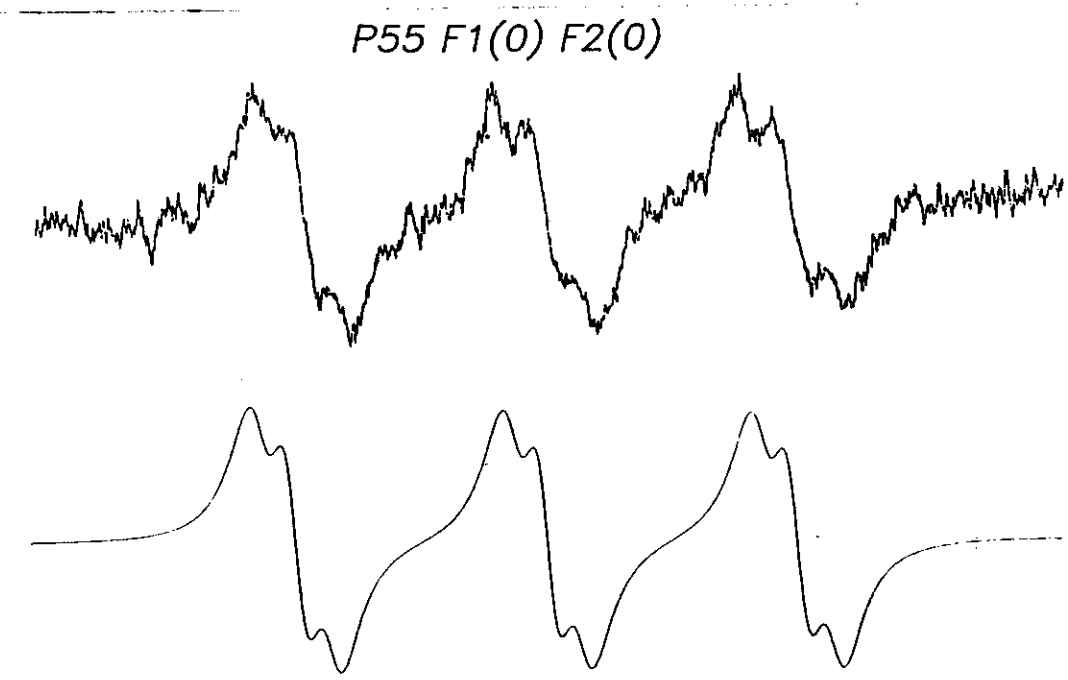

FIG II - 7